

Terrestrial Radar Observations of Dynamic Changes in Alpine Snow

Andreas Wiesmann, *Senior Member, IEEE*, Rafael Caduff, and Christian Mätzler

Abstract—Remote sensing of snow with active and passive microwaves on terrestrial, aerial, and satellite platforms has a long tradition. However, the observation of dynamic processes on alpine slopes is difficult due to fixed satellite orbits and consequently given observation geometry and interval and in some cases, also the lack of spatial resolution. Furthermore, the interferometric phase can only be used for displacement measurements if the displacement direction is more or less in the line of sight direction and the observation interval is shorter than the decorrelation time. The use of a terrestrial radar interferometer allows to overcome some of these constraints thanks to the portability of the system, the possibility to make repeat acquisitions in short intervals, and the regional observation capability. In this study, the GPRI (GAMMA portable radar interferometer, [1]) was used that is easily deployable in the field, produces images at meter scale resolution, and allows repeat acquisitions within a minute. Results of two campaigns conducted in the Swiss Alps prove the potential of terrestrial radar to measure rapid and local changes in snow parameters such as changes in the liquid water content and sudden changes in the snowpack due to skiers and avalanches. Using standard interferometric techniques, it was also possible to compute a regional snow displacement map providing information about creeping snow locations, displacement rates, and history.

Index Terms—Avalanche, interferometry, snow, snow creep, terrestrial radar.

I. INTRODUCTION

ALPINE snow is important for the regional climate, vegetation, and hydrology, but also for tourism. Furthermore, it can become a threat for infrastructure and life. Snow conditions in the Alps are dynamic and can change within minutes, as snow on the ground undergoes rapid changes such as temperature gradient metamorphism or mechanical compaction and deformation related to gravitational forces and wind.

Remote sensing of snow with active and passive microwaves has a long tradition. The sensitivity to the dielectric properties of snow and the independence of daylight and weather make the technology well suited for snow observations. Terrestrial instruments have been used to investigate the interaction of snow with microwaves at selected locations and to monitor temporal variations for model development and validation. Air- and space-borne sensors are used to image large areas

Manuscript received September 30, 2014; revised December 17, 2014; accepted January 28, 2015. Date of publication March 12, 2015; date of current version August 11, 2015.

A. Wiesmann and R. Caduff are with GAMMA Remote Sensing AG, Gümliigen CH-3073, Switzerland (e-mail: wiesmann@gamma-rs.ch; caduff@gamma-rs.ch).

C. Mätzler was with the Institute of Applied Physics University of Bern, Bern CH-3012, Switzerland. He is now with GAMMA Remote Sensing AG, Gümliigen CH-3073, Switzerland (e-mail: matzler@gamma-rs.ch).

Color versions of one or more of the figures in this paper are available online at <http://ieeexplore.ieee.org>.

Digital Object Identifier 10.1109/JSTARS.2015.2400972

and are the source for snow products such as wet snow maps [2]. However, the satellite-based instruments have a defined observation geometry and observation schedule with a repeat coverage period at best of days and fix daytime overpasses due to the polar orbits. These constraints hamper the potential to investigate dynamic processes in the snowpack spatially, especially on mountain slopes.

Portable terrestrial imaging radars, such as the GPRI (GAMMA portable radar interferometer, [1]), overcome some of these constraints. With an image acquisition time of less than 30 s and the possibility to do repeat measurements in minute intervals, they have the potential to monitor rapid processes in the snowpack. The portability allows to setup the instrument quickly and to optimize the observation geometry for the target area.

The radar image is acquired by the GPRI while rotating the antennas around the vertical axis. Image resolution is 0.9 m in range and 8 m at 1-km range in azimuth (proportional to range). The acquired radar images are complex and have phase and amplitude information per image pixel. Due to the coherent nature of the GPRI-data, investigations of the spatial distribution of the interferometric coherence with time are possible. This information can be used to track changes in the snowpack due to wind drift and melting, but also the location of free riders and changes due to avalanche release. Furthermore, the stacking of phase differences allows the production of displacement maps of the moving snow if short-time coherence is high.

II. TERRESTRIAL RADAR

The GPRI (Fig. 1) is a field-usable coherent terrestrial imaging radar operating at 17.2 GHz. The instrument has one transmit and two receive antennas (V-polarization) of about 2-m length. The focused radar image is acquired by rotating the fan-beam antennas in azimuth. A 180° image scan can be attained in less than 20 s. The system is steered by an internal controller that can operate the instrument on a preprogrammed schedule autonomously. The total instrument weight is about 35 kg and consists of carriable submodules (controller, radar unit, antennas, tower, tripod). Here, the instrument was plugged into the local 240-V power network. It can also be run from generator or a 24-V battery pack. Setup of the instrument takes less than 30 min. A more detailed description is given in [1].

III. CAMPAIGN SETUP

The instrument was setup on a boulder close to the Glogghüs ski lift station on Mägisalp (ski resort Meiringen-Hasliberg) in

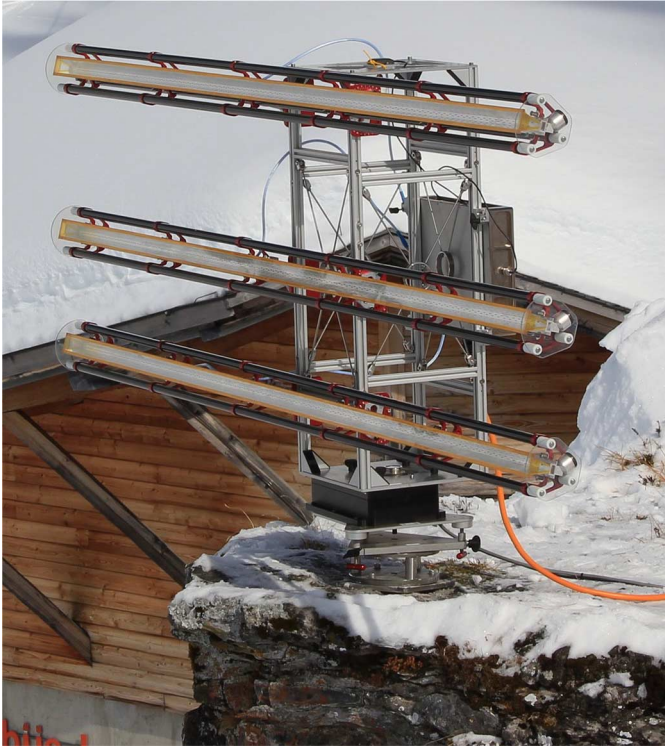
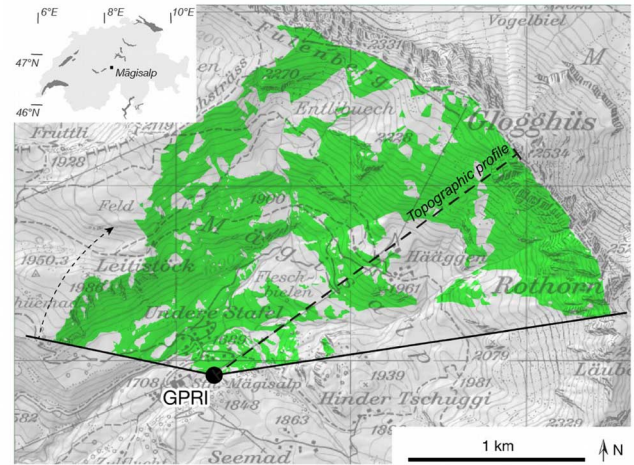


Fig. 1. GPRI mounted directly on the rock. The radar antennas rotate in azimuth and illuminate the target area in about 18 s.

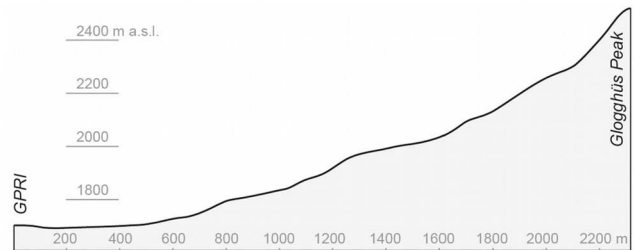
the Swiss Alps (Fig. 1). Mägisalp is located on a high plateau with alpine meadow and some sparse trees and shrubs. The setup allowed to scan the surrounding mountains of the ski resort over an azimuth angle of 170° and slant range of up to 2.5 km [Fig. 2(a)], covering altitudes from 1680 to 2530 m a.s.l. Fig. 2(b) shows the slope profile from the observation point to Glogghüs mountain peak.

Two campaigns were conducted, a first one to check the site and proof of concept on March 3, 2012 and a second one on March 27/28, 2013 for more detailed investigations. During the 2012 campaign, the weather conditions were sunny and clear sky. The snow was typical spring snow (melting conditions during sunrise, refreezing at night) with a snow height of 2.3 m at the reference spot. In March 2013, the instrument was setup in the morning of 27 March and acquisitions were stopped in the afternoon on 28 March. The snow height was 2.0 m at the reference location. The weather was again sunny but quickly turned cloudy with heavy snow fall at the end of the campaign. Due to the changing conditions, the snowpack underwent several melt–freeze cycles at the surface depending on altitude and exposition. Detailed snow profiles are shown in Fig. 3.

Images were acquired at a repeat interval of 2 min in 2012 and 3 min in 2013. During the campaign in 2013, the acquisitions were stopped at night between 00:15 and 06:00 UTC. Fig. 4 shows a radar image in radar geometry (azimuth vs. range) of the test area. Rock faces and the ski lift appear bright due to high backscatter, while shadowed areas behind trees, houses, and mounds show up dark. The photo panorama



(a)



(b)

Fig. 2. (a) Map of the test site Mägisalp, Switzerland. Green areas indicate areas illuminated by the GPRI positioned at “GPRI” (Glogghüs station). (b) Vertical profile from observation point to Glogghüs peak at 2530 m a.s.l. Map (PK50) and elevation (SwissALTI3d 5 m) swisstopo.

above the radar image is for reference. The illuminated area is indicated green in the topographic map in Fig. 2(a).

IV. DATA PROCESSING

The flowchart of the data processing chain is shown in Fig. 5. The data from the GPRI are converted to single look complex (SLC) images in radar geometry (slant range geometry). Then, the images are coregistered to a reference scene. Standard techniques are applied for the interferometric analysis using the GAMMA software suite. Orthorectification is based on the swissALTI3D 5 m DEM of swisstopo. To visualize the data on photographs, the photographs were also orthorectified using structure from motion techniques [3].

For the interferometric phase analysis, it is a prerequisite to use image pairs with high coherence, above 0.8. The coherence is a measure of the scatterer stability and thus affected by changes in the snowpack due to metamorphism, wind, and skiers, but also displacement of the snowpack. To overcome the high temporal decorrelation of snow due to metamorphism in the snowpack, images were acquired at a 2- or 3-min repeat interval. It turned out that at this interval, the interferometric coherence is usually still high and the differential phase can be interpreted as a measurable distance by which the pixel mean position has moved toward or away from the radar. From the consecutive image pairs, interferograms are computed and unwrapped. The unwrapped interferograms are then stacked,

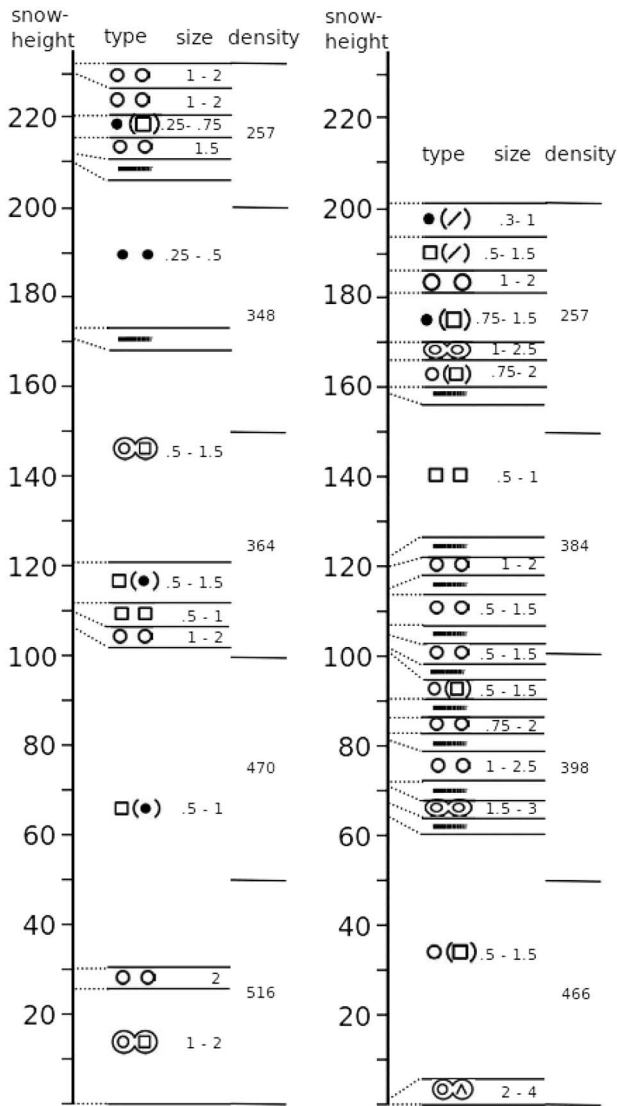


Fig. 3. Snow profiles based on WSL-SLF Davos “IHB BE Hasliberg” profiles WSL-SLF www.slf.ch. Left: March 2, 2012 09:00; right: March 30, 2013 09:00. Profiles indicate snow layers with grain type, grain diameter (in mm), and snow density (in kg/m³). Grain-type symbols are defined in [7].

and the stacked interferogram is then used to derive the displacement time series. Thanks to the high temporal sampling and strong displacement rates, no spatial or temporal filtering had to be applied. However, for shorter intervals, atmospheric effects are nominal and can be confused with the displacement signal.

V. RESULTS AND DISCUSSION

The acquired data allow to investigate the temporal and spatial behaviors of the backscattering, the interferometric coherence, and the phase changes observed. The results are presented and discussed in the following.

A. Backscattering Behavior

Fig. 6 shows the backscattering image in radar geometry of the test area of 9:03–11:03 March 27, 2013. The rock faces

aiming at, or pointing toward, the sensor show a bright signal. This is also true for slopes in the far range in the right part of the image. In the near range, the incidence angle is large and consequently only little signal is returned as indicated by the dark signature [see also the height profile in Fig. 2(b)]. Because of the distinct shadow, roads can be seen as black lines. Prepared ski slopes show a homogeneous signal and usually higher backscatter than the surrounding due to the homogeneous rough surface produced by the snow groomer.

To highlight the temporal changes spatially, the backscattering behavior in the morning, afternoon, and night of March 27, 2013 are shown in red, green, and blue, respectively, in the RGB composite in Fig. 4. Areas with persistently high backscatter during all periods show up bright. These are mainly the rock faces, but also some areas with compressed snow from older avalanches with very rough surfaces. The left side of the panorama is mainly blue, indicating stronger backscattering during the night, whereas the right side is mainly cyan, indicating stronger backscatter during the morning and the night. In fact, this reflects the frozen state of the snowpack. While the left area was already irradiated by the sun in the morning, consequently the snow surface wet, the right side was in the shadow in the morning and only illuminated in the afternoon. In the area that is already illuminated by the sun in the morning, smaller cyan areas can be seen (e.g., along the road in near range and the trees below the rock faces). These areas are due to the local topography either shaded from the sun or at very large sun incidence angle, and consequently the snow remains frozen in the morning. The snowpack on the right side only got wet after noon causing the backscatter signal to drop. Due to the smaller scale of the local topography, some areas in near range in the right part were already wet in the morning and also show the blue signature, others are bright, indicating that no snow melt happened during the day.

To get an idea about the instrument performance, an artificial target (metal plate) was used as a reference target. The signal of the reference target shows only little variations and no trend in the backscatter signal indicating good system stability. No internal calibration loop is available for the instrument calibration. Fig. 7 shows the time variation in more detail for the selected locations indicated in Fig. 6 as A and B. Location A is in the area that was illuminated by the sun already in the morning. Location B is in the area that was illuminated by the sun at around noon. The backscatter signal of location A is low in the morning and afternoon with a signal peak around noon (Fig. 7 left). During the night, the signal is again around zero and stable. While the general picture of low backscattering during the day due to wet snow and increased backscattering after refreeze is understood [4], the temporary peak at noon on 27 March must be due to changes in the snow surface structure or refroze during a short overcast. The signal of location B shows a pronounced low due to wet snow around noon on 27 March, while in the morning and later afternoon and during the night, the signal is much higher (Fig. 7 right). Smaller variations are observed during the night. The signal on 28 March differs significantly. While location A shows again the low backscatter of wet snow, location B, which is at a higher altitude, shows only a small decrease in backscatter.

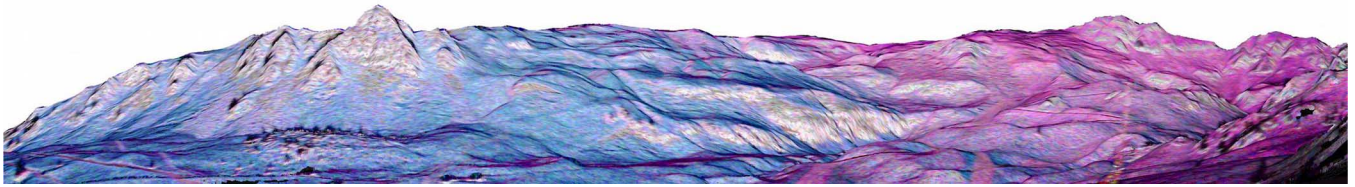


Fig. 4. RGB composite of radar backscattering (panoramic view) in the morning (red channel), afternoon (green) and night (blue) of March 27, 2013.

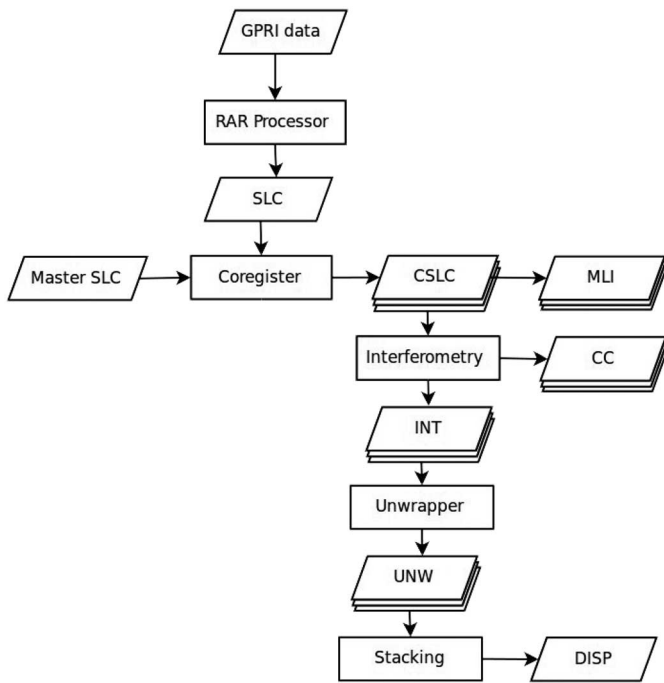


Fig. 5. Processing flowchart. SLC, single look complex; CSLC, coregistered SLC; MLI, multilook image; INT, interferogram; CC, coherence; UNW, unwrapped interferogram; DISP, displacement map.

The heavy snow fall at the end of the campaign at around noon on March 28, 2013 had a small impact on the backscatter signal. The noise level was slightly higher, visible only in shadow areas.

B. Interferometric Coherence

While the backscattering coefficient indicates the energy scattered back by the target towards the receiver, the interferometric coherence is an indicator for the stability of the scatterers in the target area between two observations. Changes in the snow structure due to snow metamorphism processes, anthropogenic, or other external mechanical impact (e.g., wind, avalanches) lead to a decrease in coherence.

Fig. 8 (left) shows the coherence image in radar geometry of the acquisition pair March 28, 2013 acquired at 9:03 and 9:06 (3-min interval). In general, the coherence after 3 min is very high. Only a few areas are decorrelated such as the trees on the left and center of the image, some ski slopes with skiers, and the ski lift. Fig. 8 (right) shows the coherence image for the

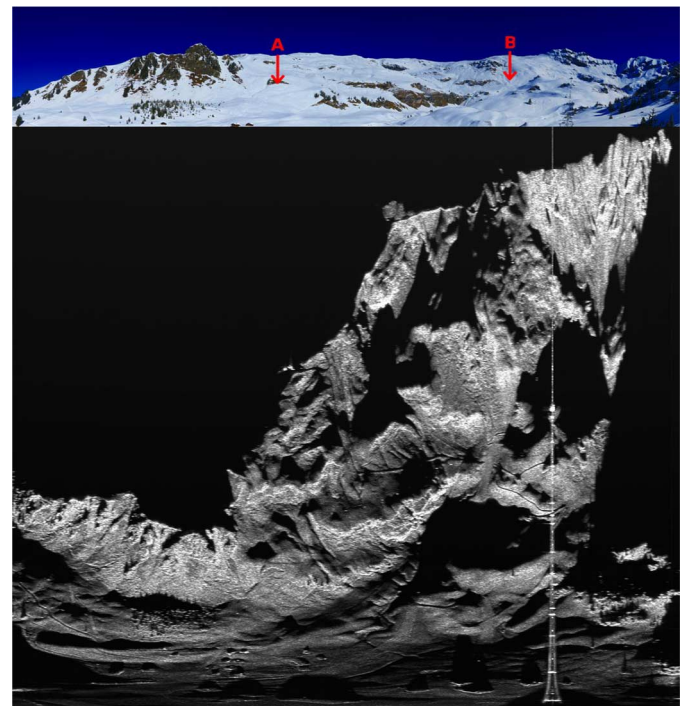


Fig. 6. Radar image in radar geometry (azimuth in horizontal direction vs. range in vertical direction) of the test area. The photo panorama above is for reference. A and B indicate target locations used in the analysis and Figs. 7, 10, and 13. Note the different scaling in distance, range (radar) versus elevation angle (photo), both March 27, 2013.

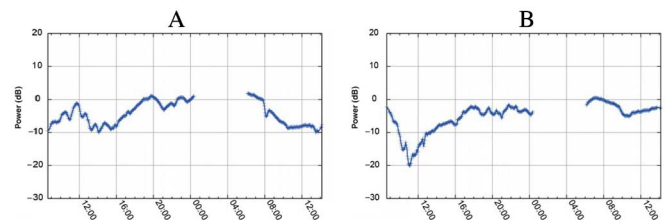


Fig. 7. Temporal behavior of the filtered backscatter signal at location A (left) and B (right) for March 27–28, 2013. A 3×3 frost filter [5] was used to reduce speckle effects.

corresponding 12-min interval (9:03 and 9:15). In addition to the areas decorrelated already after 3 min, large areas on the left part show low coherence due to the ongoing melt metamorphism. The area on the right that is still in the shade shows high coherence even after 12 min. The result stresses the need of short repeat intervals for interferometry of wet spring snow.

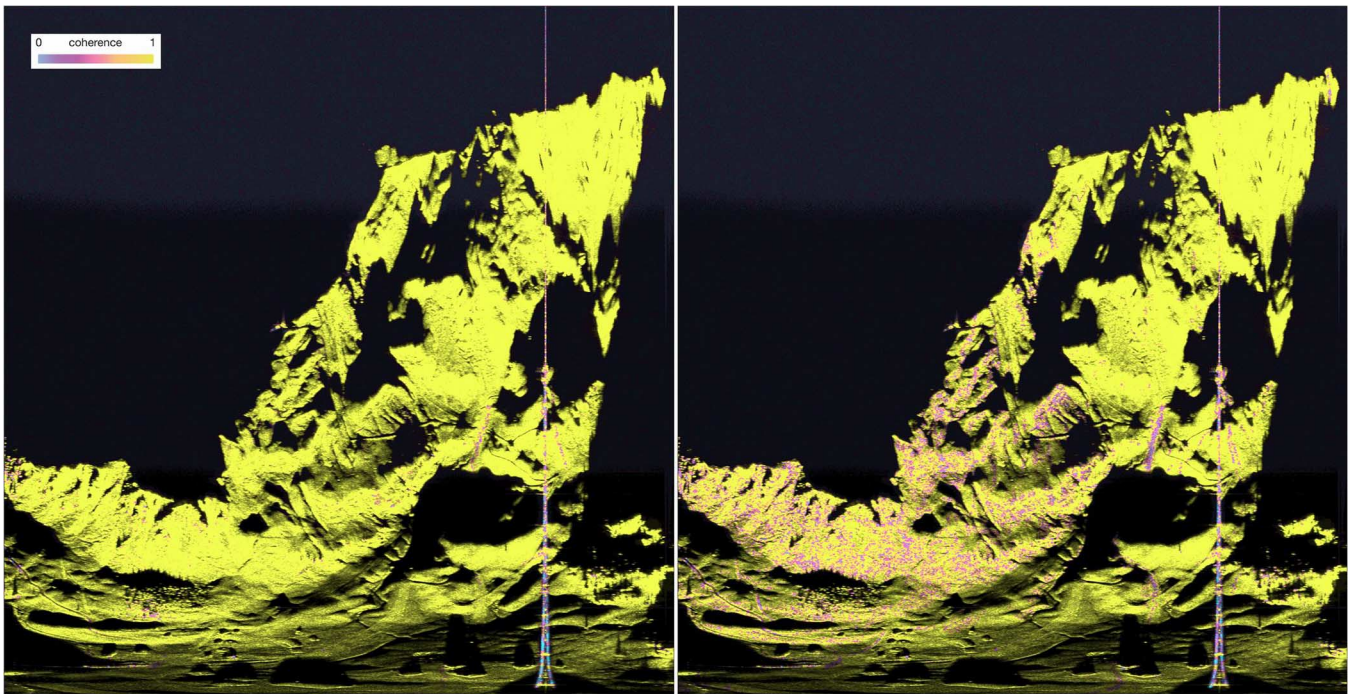


Fig. 8. Left: interferometric coherence 9:03–9:06; right: interferometric coherence 9:03–9:15 March 28, 2013 in radar geometry. Yellow indicates areas with high coherence, cyan and blue areas with low coherence. After 3 min, vegetated areas, used slopes, and the ski lift show low coherence.

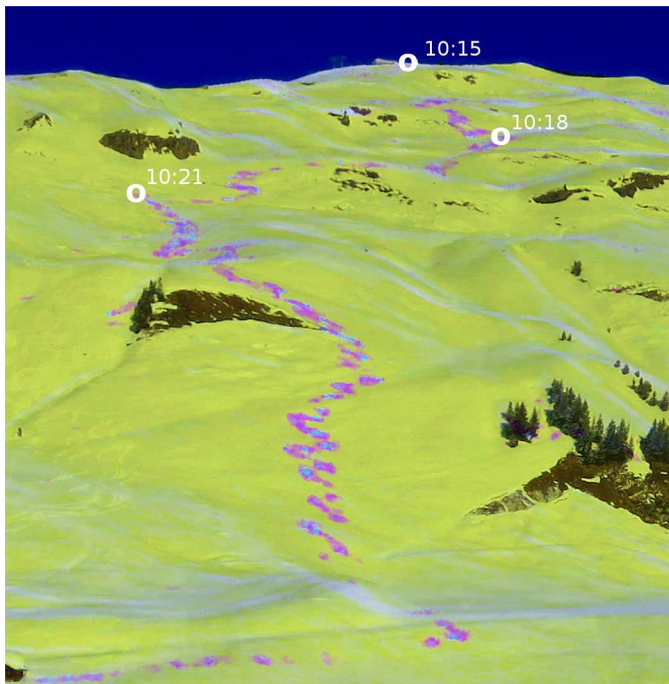


Fig. 9. Panoramic view of the coherence map. Areas with high coherence are shown in yellow. Low coherence is shown in cyan and blue. The cyan traces down the slope indicate the traces left by a free rider disturbing the snow and consequently lowering the coherence.

Fig. 9 shows a mosaic of 3-min coherence images (10:12–10:15, 10:15–10:18, 10:18–10:21, 10:21–10:24, all March 27, 2013) indicating the fresh traces of a free rider by the distinct low coherence caused in the corresponding interval image. It

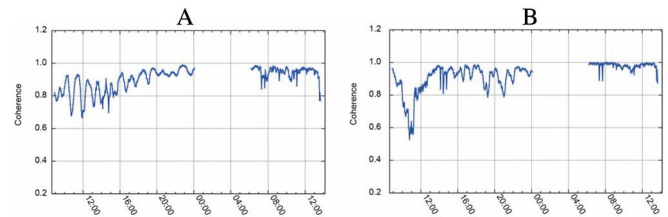


Fig. 10. Temporal behavior of the 21-min interval coherence at locations A (left) and B (right) for March 27–28, 2013. A 5×5 window was used to estimate the coherence.

must be noted that the traces could not be reliably detected in the backscatter images.

Fig. 10 shows the temporal behavior of the 21-min coherence for the same locations as for the backscattering in Fig. 7. The value is plotted at the end of the 21-min interval. The coherence of the reference target was very stable and high over the observation period. The signal at location A (Fig. 10 left) is variable during the day and varies between 0.7 and 0.9. During the evening and night as well as the 28 March, it is well above 0.9. For location B (Fig. 10 right), the signal shows a pronounced low of 0.6 at around noon on 27 March. In the afternoon, during the night and the 28 March coherence is high with two lows at 0.8 during the evening. The coherence at location B is strongly affected by the melt metamorphism observed during noon that is also visible in the backscatter signal. The coherence at location A shows a more complex pattern. The snowpack is already wet at the beginning of the experiment and less-pronounced coherence loss is observed. However, the signal is much more variable than at location B indicating changes in the snowpack within 21 min during the day. The variability of the coherence

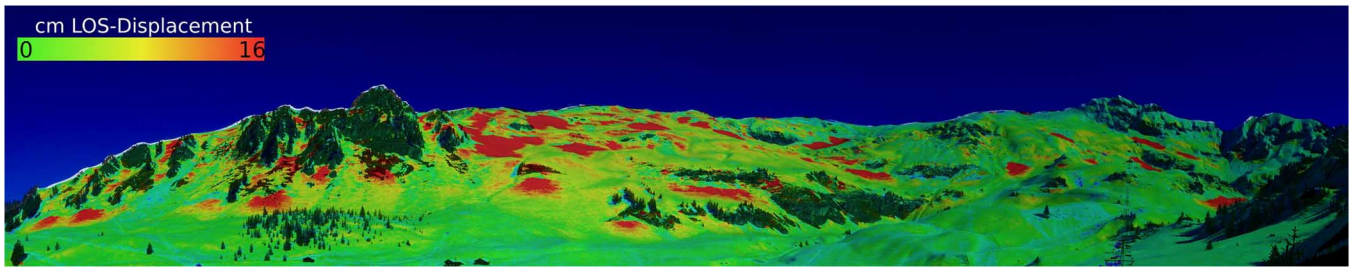


Fig. 11. Panoramic view composite of the averaged displacement rate derived from interferometric GPR data analysis for March 3, 2012. Red indicates areas that have a displacement rate of 16 cm/day or more. Green indicates areas with zero observed displacement. Background panorama photos acquired on March 27, 2013.

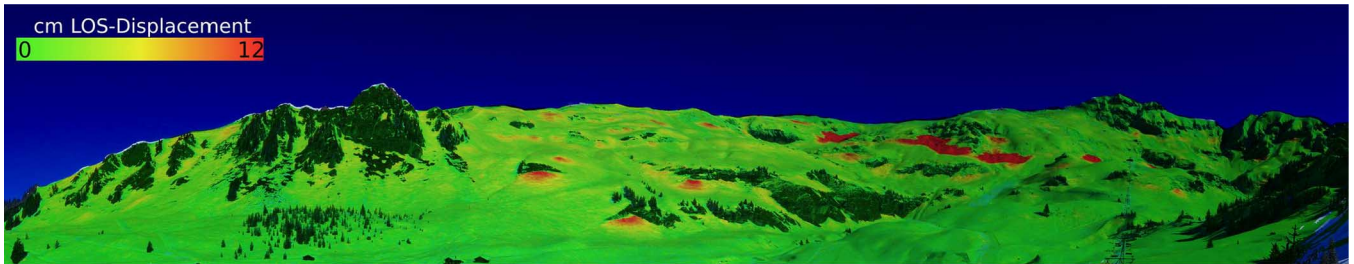


Fig. 12. Panoramic view composite of the averaged displacement rate derived from interferometric GPR data analysis for March 27/28, 2013. Red indicates areas that have a displacement rate of 12 cm/day or more. Green indicates areas with zero observed displacement. Background panorama photos acquired on March 27, 2013.

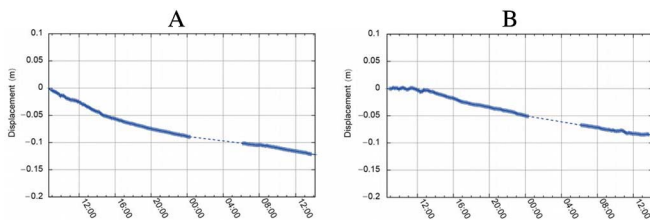


Fig. 13. Displacement history derived from interferometric phase stacking for location A (left) and location B (right) for March 27–28, 2013.

is much lower for both locations on 28 March when the sky was overcast and the snowpack close to isothermal.

C. Interferometric Phase Change (Displacement)

As indicated above, the displacement information was received from phase stacking. For both campaigns, average daily displacement rates were computed (Figs. 11 and 12). Fig. 11 shows the average displacement rates derived on March 3, 2012 on the panoramic photos acquired on March 27, 2013. Fig. 12 shows the average displacement rates derived on March 27/28, 2013 in the same geometry. Scales are slightly different to address the overall higher displacement rates in 2012. Green areas show zero displacement, whereas in red areas, a displacement of larger than 16 cm/day (2012) or 12 cm/day (2013) was observed. While the larger displacement picture is similar for the two years, variations in the exact location and rate are observed. In 2012, large-scale avalanches were observed due to large snowfall events on the unfrozen ground, leading to massive snow glides in the area. This is shown by the many hot spots observed in 2012 that are mainly linked to large glides in the snowpack and settling of older avalanche cones.

Fig. 13 shows the variability of the displacement rate with time for locations A and B for 2013. The figures indicate that the displacement rates change during the day. The displacement is larger during the day when the sun illuminates the target and smaller during the night when temperatures falls well below 0°C . For Location A, the displacement rate decreases in the afternoon (Fig. 13 left). In location B, displacement is starting only at noon on 27 March (Fig. 13 right). Unfortunately, a quantitative validation of the obtained displacement rates and changes was not possible due to the lack of validation data.

VI. CONCLUSION AND FUTURE OUTLOOK

In this paper, we have shown that terrestrial radar interferometry can provide valuable regional snow information in realtime. The backscattering information provides valuable information about the snow state, especially the presence of liquid water in the snowpack. The interferometric coherence proved to be very sensitive to sudden changes such as ski tracks, but also to changes in the snowpack due to snow metamorphism. To better understand the impact of snow metamorphism on the backscatter behavior and the coherence, more detailed ground-truth is necessary.

Finally, it was possible to derive a regional snow displacement map, indicating areas of creeping snow. Long-term campaigns will be needed to develop methodologies toward avalanche applications and also prove the method for dry winter snow.

Auxiliary information such as images of the target area and local meteorological information help in the interpretation. For the snow displacement validation-independent measurements are necessary. However, there is no established technology available to measure snow displacement spatially. At this stage,

we see best potential using time series of terrestrial photographs and tachymeter measurements of floating reflectors to validate the radar data.

The observation geometry is crucial for the success of the observation campaign. Different from satellite applications, terrestrial radar is mainly affected by shadow effects rather than foreshortening. As indicated in Fig. 2, a local DEM can be used in campaign planning to estimate the radar coverage. For displacement observations, also the line of sight has to be considered. The radar measures only the line of sight component of the displacement. See also [6] for a detailed discussion.

ACKNOWLEDGMENT

The authors would like to thank the Bergbahnen Meiringen-Hasliberg, in particular Mr. P. Michel, for the support given us during the campaigns.

REFERENCES

- [1] C. Werner *et al.*, "The GPRI multi-mode differential interferometric radar for ground-based observations," in *Proc. 9th Eur. Conf. Synth. Aperture Radar (EUSAR)*, Apr. 23–26, 2012, pp. 304–307.
- [2] T. Nagler and H. Rott, "Retrieval of wet snow by means of multitemporal SAR data," *IEEE Trans. Geosci. Remote Sens.*, vol. 38, no. 2, pp. 754–765, Mar. 2000.
- [3] R. Caduff and D. Rieke-Zapp, "Registration and visualisation of deformation maps from terrestrial radar interferometry using photogrammetry and structure from motion," *Photogramm. Rec.*, vol. 29, no. 146, pp. 167–186, 2014.
- [4] C. Mätzler and E. Schanda, "Snow mapping with active microwave sensors," *Int. J. Remote Sens.*, vol. 5, pp. 409–422, 1984.
- [5] V. S. Frost, J. A. Stiles, K. S. Shanmugan, and J. C. Holtzman, "A model for radar images and its application to adaptive digital filtering of multiplicative noise," *IEEE Trans. Pattern Anal. Mach. Intell.*, vol. 4, no. 2, pp. 157–166, Mar. 1982.
- [6] R. Caduff, F. Schlunegger, A. Kos, and A. Wiesmann, "A review of terrestrial radar interferometry for measuring surface change in the geosciences," *Earth Surf. Processes Landforms*, vol. 40, no. 2, pp. 208–228, 2014, doi: 10.1002/esp.3656.
- [7] C. Fierz *et al.*, *The International Classification for Seasonal Snow on the Ground*. IHP-VII Technical Documents in Hydrology No 83, IACS Contribution No 1, Paris: UNESCO-IHP, 2009.

Andreas Wiesmann (M'00–SM'06) received the Diploma degree in physics from the Institute of Applied Physics, University of Bern, Bern, Switzerland, in 1994 and the Ph.D. degree in physics from the same university in 1998.

Since 1998, he has been with GAMMA Remote Sensing AG, Gümüli, Switzerland. His research interests include the interaction of microwaves with natural targets, in particular snow, microwave hardware development, distributed high-performance computing, large-scale data processing, and computer security.

Rafael Caduff received the Diploma degree in earth science from the Institute of Geology, University of Bern, Bern, Switzerland, in 2008 and the Ph.D. degree in earth sciences from the same university in 2013.

Since 2013, he has been with GAMMA Remote Sensing AG, Gümüli, Switzerland. His research interests include the development, validation, and application of radar interferometry techniques for monitoring geological mass movements, including snow slope instabilities.



Christian Mätzler received the Diploma degree in physics and the Ph.D. degree in solar radio astronomy in 1970 and 1974, respectively, both from the University of Bern, Bern, Switzerland.

After Postdoctoral Research, at the Goddard Space Flight Center, National Aeronautics and Space Administration, Greenbelt, MD, USA, and at the Federal Institute of Technology (ETH), Zürich, Switzerland, he returned to the Institute of Applied Physics, University of Bern in 1978 as a Research Group Leader for terrestrial and atmospheric radiometry for remote sensing. He received his Habilitation in applied physics with emphasis on remote sensing methods in 1986 and the title of a Titular Professor in applied physics and remote sensing in 1992. He spent sabbaticals in 1996 with the University of Colorado, Denver, CO, USA, and with the University of Washington, Seattle, WA, USA, and in 2004, with the Paris Observatory, Paris, France. In July 2010, he retired from the university. Currently, he is a Consultant for Gamma Remote Sensing, Gümüli, Switzerland. His research interests include microwave (1–100 GHz) signatures for active and passive remote sensing of the atmosphere, snow, ice, soil, and vegetation, as well on the development of methods for dielectric and propagation measurements for such media. He is the Editor of a book *Thermal Microwave Emission With Applications For Remote Sensing*.